Acta Crystallographica Section D
Biological Crystallography
ISSN 0907-4449

Structures of *Plasmodium falciparum* purine nucleoside phosphorylase complexed with sulfate and its natural substrate inosine

Claudia Schnick,[a]‡ Mark A. Robien,[b]‡ Andrzej M. Brzozowski,[a] Eleanor J. Dodson,[a] Garib N. Murshudov,[a] Lori Anderson,[b] Joseph R. Luft,[c] Chris Mehlin,[b] Wim G. J. Hol,[b]* James A. Brannigan[a]* and Anthony J. Wilkinson[a]

[a]Structural Biology Laboratory, Department of Chemistry, University of York, York YO10 5YW, England, [b]Structural Genomics of Pathogenic Protozoa (SGPP), Department of Biochemistry, Biomolecular Structure Center, University of Washington, Seattle, Washington 98195, USA, and [c]SGPP, Structural Biology Department, Hauptman–Woodward Medical Research Insitute, 73 High Street, Buffalo, New York 14203, USA

‡ These authors contributed equally.

Correspondence e-mail: wghol@u.washington.edu, jab@ysbl.york.ac.uk

© 2005 International Union of Crystallography
Printed in Denmark – all rights reserved

Received 6 June 2005
Accepted 28 June 2005

PDB References: *Pf*PNP–ino, 2bsx, r2bsxsf; *Pf*PNP–SO_4, 1sq6, r1sq6sf.

Purine metabolism in the parasite *Plasmodium* has been identified as a promising target for antimalarial therapies. Purine nucleoside phosphorylase (PNP) is part of a salvage pathway for the biosynthesis of purines, which are essential for parasite survival. Two crystal structures of PNP from *Plasmodium falciparum* (*Pf*PNP) in two space groups, each with a single subunit in the asymmetric unit, are described here. One structure, refined to 2.4 Å, has an empty nucleoside-binding site and a sulfate ion bound in the phosphate-binding pocket. The second structure, refined to 2.0 Å, has the substrate inosine bound to the active centre. Structure comparison reveals alterations in the active site upon ligand binding. The new structures presented here specifically highlight the likely roles of Asp206 and two loops flanking the active site: the β_7-α_6 loop (residues ∼161–169) and the β_9-α_8 loop (residues ∼208–223). Comparison with PNP in complex with transition-state inhibitors suggests that the purine substrate moves towards the phosphate substrate, rather than *vice versa*, upon forming the transition state. The single-substrate-containing *Pf*PNP structures also appear to be more flexible than *Pf*PNP bound to inhibitors. Together, these structures serve as a basis for better understanding of ligand binding and mechanism that can be further exploited to optimize the specificity of anti-*Pf*PNP drugs.

1. Introduction

Malaria is caused by the single-celled protozoan parasite *Plasmodium*, which infects host liver and red blood cells and is transmitted through the bite of the female *Anopheles* mosquito. About 40% of the world population is at risk of malaria, with an estimated 300 million acute cases every year, most of them in tropical Africa (Suh *et al.*, 2004). Of the four *Plasmodia* species that are infectious to humans, *P. falciparum* is responsible for the most serious disease, inducing anaemia, organ failures and coma. With an estimated one to three million people dying of malaria every year and the capacity of the parasite (i) to develop resistance to antimalarials and (ii) to evade the host's immune response by antigenic variation, it is clear that there is an urgent need to find novel targets for new drugs against this disease.

Purine metabolism in *P. falciparum* has been identified as a promising target for antimalarials since it is distinct from that of humans. In contrast to humans, *Plasmodia* species are purine auxotrophs; that is, they cannot synthesize purines *de novo* (Hassan & Coombs, 1988). To guarantee a supply of purines for RNA and DNA synthesis during cell growth, the parasite is dependent on a salvage pathway that utilizes nucleosides obtained from the host. The enzyme purine nucleoside phosphorylase (PNP) plays an important role in

this pathway (Fig. 1). It catalyzes the phosphorolysis of inosine to ribose-1-phosphate and hypoxanthine, which is the primary purine precursor for the salvage pathway (Asahi *et al.*, 1996). Inosine itself is produced by the deamination of adenosine, which is the major purine nucleoside in human blood. The importance of PNP for parasite survival has been shown in experiments with transition-state analogues that block enzyme activity and cause purine-less cell death (Kicska, Tyler, Evans, Furneaux, Kim *et al.*, 2002; Kicska, Tyler, Evans, Furneaux, Schramm *et al.*, 2002).

Owing to its importance as a therapeutic target, PNPs from a wide range of organisms have been investigated. The structure and function of PNP is conserved among organisms from bacteria to eukaryotes, even though the sequence identity is often low (Pugmire & Ealick, 2002). The subunit fold of PNPs is similar to that of functionally related enzymes such as 5′-methylthioadenosine phosphorylase (MTAP) and uridine nucleosidase. According to this shared subunit fold, these enzymes have been assigned to the nucleoside phosphorylase I family (Pugmire & Ealick, 2002). Although the tertiary structure is strongly conserved, the quaternary structure is variable, with hexamers prevalent in bacteria such as *Escherichia coli*, *Vibrio cholerae* and *Thermus thermophilus*, while trimers prevail in more highly developed organisms such as mammals.

The substrate specificity of PNPs from different origins seems to correlate with the two categories of quaternary structure. The trimeric forms are active towards 6-oxopurine nucleosides, whereas the hexameric forms utilize a wider range of substrates including 6-aminopurine nucleosides. The difference in substrate specificity between human and *E. coli* PNP has already been explored in gene-therapy treatments: prodrugs that cannot be cleaved by the human enzyme can be activated by *E. coli* PNP expressed in tumour cells and converted to toxic bases which kill the tumour tissue (Parker *et al.*, 1997).

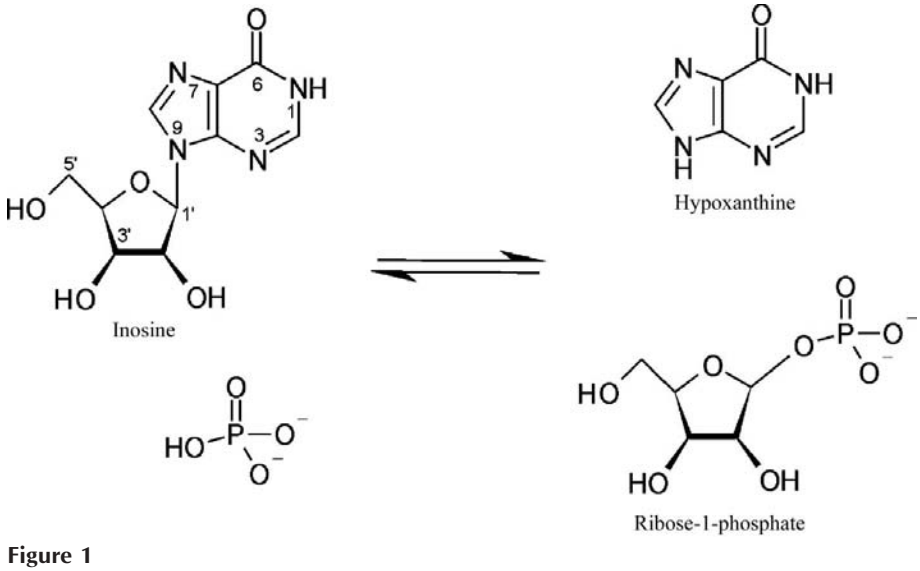

Figure 1
Phosphorolysis of inosine catalysed by *P. falciparum* PNP. The product hypoxanthine is the major precursor for the purine-salvage pathway.

The substrate specificity of the malarial PNP has been tested on several nucleosides (Kicska, Tyler, Evans, Furneaux, Kim *et al.*, 2002). In contrast to most hexameric PNPs, *Plasmodium* PNP accepts 6-oxopurines such as inosine and guanosine, but not the 6-aminopurine adenosine. Surprisingly, this substrate specificity is reminiscent of trimeric mammalian PNPs. Also in contrast to other PNPs, the malarial enzyme is active towards the pyrimidine nucleoside uridine. This matches its phylogenetically unique position, which is equidistant in sequence from the majority of PNPs and the uridine phosphorylases (Kicska, Tyler, Evans, Furneaux, Kim *et al.*, 2002).

Here, we present the three-dimensional structures of PNP from *P. falciparum* with sulfate bound to the active site (PNP–SO_4) and in complex with inosine (PNP–ino). In combination with those of the enzyme in complex with immucillins (Shi *et al.*, 2004), these structures provide detailed insights into the enzyme's chemistry and specificity which may be exploited for the design of novel compounds or to optimize existing inhibitors.

2. Materials and methods

2.1. Cloning and expression of *P. falciparum* PNP

The coding sequence for PNP from *P. falciparum* strain 3D7 (*Pf*PNP) was amplified by polymerase chain reaction (PCR) using genomic DNA as a template. Primers complementary to the gene with the PlasmoDB accession code PFE0660c were designed which flank the 5′ and 3′ ends of the amplified fragment with recognition sites for the restriction enzymes *Nco*I and *Xho*I, respectively. The sequence of the sense primer was 5′-TCATCCATGGATAATCTTTTACGCCATTTAAAAATCAGCAAGGAAC-3′ and that of the antisense primer was 5′-CACACTCGAGGGCATATTTGGTTGCTAATTTTGCACATG-3′. The PCR cycling parameters were denaturation at 367 K (0.5 min), annealing at 318 K (0.5 min) and extension at 338 K (2 min), repeated over 28 cycles. Following restriction-enzyme digestion, the amplified PCR fragment was ligated into *Nco*I/*Xho*I-cut pET28a (Novagen) plasmid DNA, producing a construct that encodes *Pf*PNP with a His_6 tag at its C-terminus.

The plasmid was introduced into the *E. coli* expression strain BL21-CodonPlus (Stratagene). For protein preparation, cultures were grown in LB medium supplemented with 50 µg ml^{-1} chloramphenicol and 30 µg ml^{-1} kanamycin. When the OD_{600} reached 0.5, expression of recombinant protein was induced by the addition of isopropyl-β-D-thiogalactopyranoside (IPTG) to 1 m*M* final concentration and cells were incubated for a further 4 h at

303 K. The cells were pelleted by centrifugation and stored at 253 K.

The gene was also cloned into pET14b (Novagen), providing it with an N-terminal His_6 tag for the *Pf*PNP–SO_4 studies. For expression, *E. coli* strain BL21-Star (DE3) (Invitrogen) was used. Cell cultures (1 l) were grown at 310 K in M9 minimal medium supplemented with 100 µg ml^{-1} ampicillin, with the incubation temperature progressively reduced to 291 K at an OD_{600} = 0.1–0.3. When the OD_{600} reached 0.4, the culture was supplemented with 40 ml of an amino-acid mixture containing 125 mg of lysine, threonine and phenylalanine and 65 mg of leucine, isoleucine, valine and selenomethionine after the method of Van Duyne *et al.* (1993). Expression of recombinant protein was induced by the addition of IPTG to a final concentration of 0.5 m*M* 30 min later. Cells were incubated overnight, harvested by centrifugation and stored at 195 K.

2.2. Purification of PNP

Cells for the *Pf*PNP–ino studies were resuspended in 5 ml 50 m*M* NaH_2PO_4 pH 8.0, 300 m*M* NaCl (buffer *A*) per gram of cell pellet. Lysozyme was added to the cell suspension to 1 mg ml^{-1} and the suspension was incubated on ice for 30 min before sonication. The cell debris was removed by centrifugation for 20 min at 10 000*g* at 277 K. The cleared cell lysate was incubated with equilibrated Ni–NTA resin (Qiagen) for 60 min on a rotary shaker at 277 K. The Ni–NTA resin was poured into a column and washed with 10 m*M* imidazole in buffer *A*. His-tagged PNP was eluted with a linear gradient of 25–150 m*M* imidazole in buffer *A*. Fractions were analyzed by SDS–PAGE and those that showed a prominent band corresponding to a molecular weight of ∼28 kDa were pooled and applied onto a Hi-Load Superdex 200 16/60 gel-filtration column (Amersham Biosciences) equilibrated with buffer *A*. Pure *Pf*PNP eluted as a single peak from this column as confirmed by Coomassie-stained SDS–PAGE analysis. The enzyme was stored at 277 K.

Cells for the *Pf*PNP–SO_4 studies were resuspended in 20 ml 20 m*M* HEPES pH 7.5, 5%(*v*/*v*) glycerol, 1 *M* NaCl and 2 m*M* β-mercaptoethanol. Using this buffer, the protein was purified by Ni–NTA and subsequent gel-filtration chromatography in a similar manner as described for the *Pf*PNP–ino protein.

2.3. Analytical ultracentrifugation

The molecular weight of PNP was determined by analytical ultracentrifugation in a Beckman Optima XL/I centrifuge (AN60Ti rotor) using Beckman cells with 12 mm path length, six-channel charcoal-filled Epon centrepieces and quartz windows. PNP samples of ∼2 mg ml^{-1} and serial twofold dilutions thereof were analysed in sedimentation-equilibrium experiments at 293 K with a cell containing 50 m*M* NaH_2PO_4 pH 8.0, 300 m*M* NaCl as a reference. Absorbance scans were taken at 3000 rev min^{-1} to check loading concentrations and uniform distribution in the cells. The speed was increased to 10 000 and 13 000 rev min^{-1}, respectively, and absorbance scans were taken at 4 h intervals until sedimentation equilibrium was achieved. Scans were conducted in step mode with ten replicates per data point; data were recorded at 280 nm and at 295 nm. The Beckman *Origin* data-analysis package was applied to calculate the molecular weight of the PNP sample by fitting model curves to the experimental data.

2.4. Activity assays

The activity of purified *Pf*PNP towards various substrates present at 0.15 m*M* was determined photometrically in 50 m*M* NaH_2PO_4 buffer pH 7.5. The enzyme concentration was adjusted so that substrate conversion was linear with respect to time. This continuous assay was used to calculate the rate of substrate conversion per milligram of protein from the initial linear part of the reaction curve. Activity against inosine was tested in a coupled assay in which the reaction mix contained 0.16 units ml^{-1} of xanthine oxidase, which converts hypoxanthine formed by PNP to uric acid. The reaction time course was measured by monitoring the increase of uric acid concentration at 293 nm (ε = 12.9 mM^{-1} cm^{-1}). The substrate 2-amino-6-mercapto-7-methylpurine (MESG), which is a component of the EnzCheck phosphate-assay kit (Molecular Probes), was assayed by monitoring the increase in absorbance at 360 nm (ε = 11 mM^{-1} cm^{-1}). Uridine phosphorylase activity was measured by incubating *Pf*PNP with uridine and monitoring the increase in absorbance at 290 nm (ε = 5.41 mM^{-1} cm^{-1}) arising from the uracil product.

2.5. Crystallization and data collection

For crystallization of C-terminally His_6-tagged *Pf*PNP in complex with inosine, the protein-storage phosphate buffer was exchanged for 0.1 *M* HEPES pH 7.5, 0.1 *M* NaCl and the protein was concentrated to 5 mg ml^{-1}. Crystals were obtained by the hanging-drop method. 1 µl protein solution was mixed with an equal volume of reservoir solution containing 10%(*w*/*v*) PEG 8000, 0.1 *M* HEPES pH 7.5, 30%(*v*/*v*) hexanetriol and 10 m*M* inosine. The drops were equilibrated by vapour diffusion against 0.5 ml of the corresponding reservoir solution at 293 K. Crystals of hexagonal shape appeared after 1–3 d. Crystals of PNP were grown in the presence of 10 m*M* uridine (PNP–uri) following the same procedure. For data collection, the crystals were mounted in nylon loops and flash-cooled in a stream of nitrogen gas at 100 K. Data sets were collected on beamlines ID29 and ID14.1 at the European Synchrotron Radiation Facility. The data were indexed and scaled with the programs *DENZO* and *SCALEPACK* (Otwinowski & Minor, 1997). Extreme anisotropy made processing and scaling at higher resolution very difficult; however, rather than truncate the data to 2.4 Å resolution, it was decided to attempt to exploit the complete diffraction. Using this incomplete higher resolution data certainly improved the electron density.

Crystals of the N-terminally His_6-tagged enzyme used for the *Pf*PNP–SO_4 studies were grown by the sitting-drop technique in a buffer composed of 25%(*w*/*v*) PEG 3350, 0.1 *M* ammonium sulfate and 100 m*M* MOPS pH 6.5 at 293 K. A single-wavelength data set from this crystal was collected at

the selenium-peak absorption energy of 0.9795 eV at beamline 8.2.1 at the Advanced Light Source. The data were indexed and scaled with the programs *DENZO* and *SCALEPACK* (Otwinowski & Minor, 1997).

2.6. Structure determination and refinement

For the *Pf*PNP–ino structure, a clear and unambiguous molecular-replacement solution was obtained with a monomer of *E. coli* uridine phosphorylase (PDB code 1lx7; Burling *et al.*, 2003) as the search model using *MOLREP* (Vagin & Teplyakov, 1997) from the *CCP*4 suite (Collaborative Computer Project, Number 4, 1994). The crystallographic symmetry operators applied to this solution generated a hexamer with satisfactory intramolecular and intermolecular contacts. The initial electron-density maps calculated after rigid-body refinement of the model allowed corrections of the amino-acid sequence to be made, and several missing fragments of the main chain to be traced.

However, refinement trials of the model using routine protocols implemented in *REFMAC*5 (Murshudov *et al.*, 1997) were unsuccessful, with the $R_{\rm free}$ parameter trapped close to its starting value of 50%. Several refinement options were attempted, with an anisotropic scaling approach giving the best results. Although much of it is very weak, use of all the data in the highest resolution shells was essential for the refinement and model building of the structure. Automatic model building using *ARP*/*wARP* (Perrakis *et al.*, 1999) failed; however, the *ARP*/*wARP* free-atoms update procedure was used after the removal of all suspect residues outside electron density. Iterative cycles of this procedure plus refinement with *REFMAC*5 and careful manual model building were performed. After 10–20 rounds of model building and refinement, the procedure ceased to improve the phases. TLS parameterization (Howlin *et al.*, 1993) attempted towards the end of refinement surprisingly failed to improve the statistics when all data were used. Instead, refinement began to misbehave. To see if this behaviour persisted at various resolutions, the TLS parameterization was attempted with various resolution cutoffs. When the data were truncated to 2.5 Å, TLS refinement did indeed improve the statistics for the *Pf*PNP–uri data set, with a resulting R factor of 17.7% ($R_{\rm free}$ = 25.0%) compared with a starting R factor of 18.7% ($R_{\rm free}$ = 26.3%), indicating that the parameterization was sensible. Statistics for all data with these TLS parameters resulted in an R factor of 21.9% ($R_{\rm free}$ = 26.5%). However, the R factor for all data for *Pf*PNP–ino remained unusually high at 26.8% ($R_{\rm free}$ = 34.2%). The R factor for data truncated to 2.4 Å was 20.8% ($R_{\rm free}$ = 30.1%). One of the reasons for this behaviour could be the inaccurate conversion of intensities to structure factors. A representation of the diffraction anisotropy is provided as supplementary material.[1]

For the *Pf*PNP–SO_4 structure, four Se sites were found using *SOLVE*/*RESOLVE* (Terwilliger & Berendzen, 1999) and an initial trace of the protein backbone was obtained by fitting a monomer of the *E. coli* PNP into the resulting phased density using *MOLREP*. Despite the experimental phasing and nominal medium resolution, the progress of the *REFMAC*5 refinement of the *Pf*PNP–SO_4 structure was seemingly hampered by the serious anisotropy of the structure factors, similar to the problems noted above for the *Pf*PNP–ino structure. H atoms were added in their riding positions and a few cycles of refinement with anisotropic scaling were carried out. For the final model, all attempts to include residues 208–223 in the extremely weak density seen in this region were abandoned, resulting in a final R factor for all data to 2.4 Å of 18% and an $R_{\rm free}$ of 26%. The final models comprise residues 4–207 and 224–244 (*Pf*PNP–SO_4), 1–214 and 221–247 (*Pf*PNP–ino), 2–210 and 221–244 (*Pf*PNP–uri).

3. Results and discussion

3.1. Cloning and purification of *Pf*PNP

The sequence of the single exon gene encoding *Pf*PNP was identified in the *Plasmodium* genome database PlasmoDB (http://www.plasmodb.org), where it is annotated as a putative uridine phosphorylase. This annotation stems from the fact that it is equidistant in sequence between uridine phosphorylases and purine nucleoside phosphorylases (Kicska, Tyler, Evans, Furneaux, Kim *et al.*, 2002). A *BLAST* search reveals 28% protein sequence identity with the *E. coli* uridine phosphorylase and 30% identity with *E. coli* PNP.

The open reading frame encoding the 245-amino-acid residue *Pf*PNP (PlasmoDB accession code PFE0660c) was amplified from *P. falciparum* 3D7 genomic DNA and cloned into an *E. coli* expression vector alongside sequences specifying either a C-terminal or an N-terminal His_6 tag. DNA sequencing was used to confirm the authenticity of the expression constructs. Induction of expression produced soluble recombinant protein, which was purified by Ni–NTA and gel-filtration chromatography. The subunit molecular weight of the expressed and tagged protein is calculated to be 27.9 kDa, which corresponds well to that of the single protein band ($M_{\rm app}$ = 25–30 kDa) observed by denaturing gel electrophoresis after purification.

3.2. Biochemical characterization of purified *Pf*PNP

To determine the subunit composition of recombinant *Pf*PNP, its sedimentation coefficient was measured by ultracentrifugation in a sedimentation-equilibrium experiment. The determined sedimentation coefficient of 7×10^{-13} s allowed the molecular weight to be estimated as 160 kDa. As the molecular weight of the monomer is 27.9 kDa, this corresponds most closely to a hexamer (167.4 kDa). This agrees with the hexamer observed in the crystal structure of the immucillin-complexed PNP from *Plasmodium* (Shi *et al.*, 2004) and reiterates the unique characteristics of the malarial PNP in comparison to other members of the PNP family, where hexameric assemblies are more typical of bacterial organisms than eukaryotes.

[1] Supplementary material has been deposited in the IUCr electronic archive (Reference: GX5066). Services for accessing these data are described at the back of the journal.

Table 1
Qualitative assay for activity of the purified recombinant *Pf*PNP at saturating substrate concentrations.

Substrate	Substrate conversion (μmol mg $^{-1}$ min^{-1})	Activity (%)
Inosine	3.67 ± 0.18	100
MESG	3.98 ± 0.32	108
Uridine	0.32 ± 0.012	8.7

*Pf*PNP activity was examined as a further test of the integrity of the purified recombinant enzyme. The turnover of three different substrates at fixed saturating concentrations was tested, these being the natural substrate inosine, a guanosine analogue (MESG) and uridine. A continuous assay showed qualitatively that substrate-conversion rates for the two 6-oxopurines, inosine and MESG, were similar and approximately an order of magnitude greater than that for uridine (Table 1). The fact that uridine is turned over by *Pf*PNP shows a functional similarity to the uridine phosphorylases, even though purines are clearly the preferred substrates. A similar activity ratio of inosine/uridine has been previously quantified, where the k_{cat} for uridine was determined to be 7.6% of that measured for inosine (Kicska, Tyler, Evans, Furneaux, Kim *et al.*, 2002). Adenosine was not tested here, since it is not a substrate for the malarial PNP. In this regard, the substrate specificity of hexameric *Pf*PNP more closely resembles that of the trimeric human enzyme, which is active against 6-oxopurines but not 6-aminopurines, whereas hexameric bacterial PNPs such as the *E. coli* enzyme have a broader substrate specificity that embraces adenosine (Pugmire & Ealick, 2002).

Table 2
Crystal parameters and statistics of data collection, refinement and model quality.

Values in parentheses are for the last shell. Note the similarity of the cell dimensions between the two crystal space groups.

	*Pf*PNP–uri	*Pf*PNP–ino	*Pf*PNP–SO_4
Data collection			
Space group	*H*32	*P*321	*H*32
Unit-cell parameters (Å)	*a* = 95.45, *b* = 95.45, *c* = 135.78	*a* = 95.12, *b* = 95.12, *c* = 47.08	*a* = 95.09, *b* = 95.09, *c* = 134.79
Resolution (Å)	30.0–1.8 (1.86–1.8)	20.0–2.0 (2.07–2.0)	28.26–2.4 (2.53–2.4)
No. of reflections	21910	27984	7135
Data redundancy	9.0 (8.2)	2.5 (2.4)	8.0 (3.5)
Completeness (%)	99.4 (96.3)	87.0 (80.0)	78.3 (43.1)
R_{sym}	0.043 (0.258)	0.082 (0.348)	0.129 (0.291)
$I/\sigma(I)$	10.0 (3.0)	10.0 (5.0)	10.1 (3.8)
Refinement			
R factor	0.219	0.268 [0.208]†	0.184
R_{free}	0.265	0.342 [0.301]†	0.265
No. of amino acids	233	241	225
No. of ligands	—	1 inosine	1 SO_4
No. of waters	120	105	48
Average *B* factor (Å^2)	38.2	38.8	32.4
Wilson *B* factor‡ (Å^2)	40.5	40.2	58.9
R.m.s. deviations			
Bond (Å)	0.017	0.018	0.010
Angle (°)	1.51	1.93	1.27
Ramachandran plot (%)			
Favoured regions	87.6	84.3	88.3
Additional allowed	11.9	13.8	10.7
Generously allowed	0.5	1.4	1.0
Disallowed	0	0.5	0

† The value in square brackets is the *R* factor for data with a high-resolution cutoff at 2.4 Å. ‡ Overall Wilson *B* values estimated from data truncated to 2.4 Å are compromised by the anisotropic data (see supplementary material).

3.3. *Pf*PNP crystals and overall structure

Two different and independently refined *Pf*PNP structures are presented here. The first is refined against markedly anisotropic data extending to 2.4 Å, in which no nucleoside is bound, although a sulfate ion was located in the active site (*Pf*PNP–SO_4). This structure was determined from crystals grown in space group *H*32. The second structure has been refined against 2.0 Å resolution data and is of the inosine-liganded enzyme (*Pf*PNP–ino). The crystals of *Pf*PNP–ino belong to space group *P*321 (Table 2). The packing of the hexameric discs in the *ab* planes are the same but there is shearing perpendicular to the *c* axis, which generates a different space group and probably contributes to the anisotropy. The asymmetric unit in both crystals is a monomer.

A third data set was acquired from a crystal of *Pf*PNP grown in the presence of uridine (*Pf*PNP–uri). This crystal, also in space group *H*32, was isomorphous to the first structure described and diffracted to 1.8 Å resolution in the *ab* plane, but to an approximate resolution of 3.0 Å in the weak direction. This data set was used concurrently with the *Pf*PNP–ino data set to complement the refinement strategy. Model building and refinement was hampered by the extremely high anisotropy in the data, which is reflected in the high *R* factors (see supplementary material). Despite this, the electron-density maps are of good quality overall (Figs. 2*a* and 2*b*). The inosine ligand in the *Pf*PNP–ino complex is well defined; however, the occupancy of the uridine ligand in the *Pf*PNP–uri complex is low and the electron-density maps do not allow the ligand to be modelled with any confidence. The low occupancy is presumably a consequence of the ∼17-fold lower affinity binding of uridine relative to inosine (Kicska, Tyler, Evans, Furneaux, Kim *et al.*, 2002).

The *Pf*PNP–ino model comprises residues 1–214 and 221–245 of the native enzyme with two additional residues (Leu-Glu) at the C-terminus introduced during the cloning procedures. The electron-density maps failed to define residues 215–220, which are assumed to be disordered. 105 water molecules and one inosine molecule, bound at the active site, were identified in the maps. There was no evidence for the presence of an anion in the phosphate-binding site. The Ramachandran plot for this model shows one residue (Arg45) with defined electron density in a disallowed region.

The *Pf*PNP–SO_4 structure was solved in an anomalous dispersion experiment following selenomethionine incorporation into the protein. Refinement resulted in an *R* factor of 18.4% with an R_{free} of 26.5%. This model includes residues 4–207 and 224–244 of the PNP primary sequence, with a discontinuity of 16 residues that could not be built. 48 waters were identified along with one sulfate ion that occupies the phosphate-binding site of the enzyme, while its nucleoside-

binding site is empty. Similar to the *Pf*PNP–ino structure as well as the immucillin-bound *Pf*PNP structures, a generously allowed residue in the Ramachandran plot for *Pf*PNP–SO_4 is again Arg45, which is implicated in the catalytic mechanism (see below). This is in accordance with the general observation that steric strain tends to correlate with functional significance (Herzberg & Moult, 1991).

Superposition of the *Pf*PNP–SO_4 structure with the inosine-complexed structure (Fig. 2*c*) produces a root-mean-square deviation of 0.37 Å on the positions of equivalent main-chain C^{α} atoms and shows that there are no major conformational differences in the overall fold of the enzyme. The *Pf*PNP polypeptide chain folds to form a single-domain subunit with a core of nine β-strands surrounded by eight α-helices (Figs. 2*c* and 3*b*). The β-strands are arranged in two sheets with an N-terminal four-stranded β-sheet (β_2-β_3-β_4-β_1) merging into a C-terminal five-stranded β-barrel-like structure (β_5-β_9-β_6-β_7-β_8).

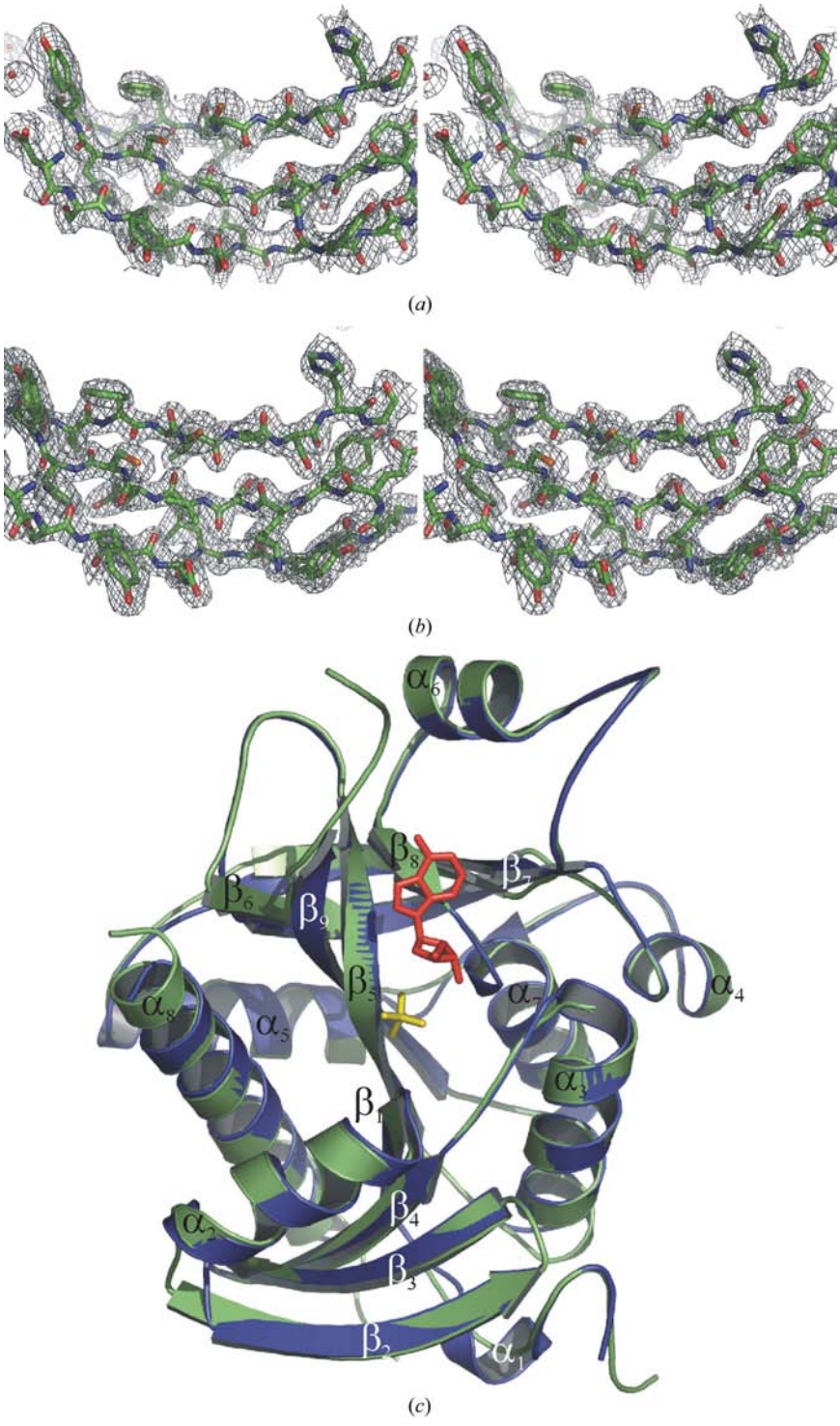

Figure 2
Overall structure of the *Pf*PNP subunit. (*a*) Section of the stick model coloured by atom of *Pf*PNP–ino with electron density displayed (omit map) at 0.5σ. (*b*) Section of the model of *Pf*PNP–ino with $2F_o - F_c$ electron density displayed at 1.0σ. (*c*) Superposition of the *Pf*PNP–ino structure (light green) and the *Pf*PNP–SO_4 structure (blue). Inosine is shown in red and sulfate in yellow. This and subsequent figures were generated using *PyMol* (DeLano, 2002).

3.3.1. Quaternary structure. The quaternary arrangement of *Pf*PNP is similar to those of the PNPs from *E. coli* (PDB code 1ecp; Mao *et al.*, 1997), *V. cholerae* (PBD code 1vhj; Structural Genomix, unpublished work) and *T. thermophilus* (PDB code 1odi; Tahirov *et al.*, 2004) as well as that of MTAP from *Sulfolobus solfataricus* (PDB code 1je1; Appleby *et al.*, 2001). The disc-shaped hexamer has an overall diameter of about 100 Å and a central channel with a diameter of 20 Å (Fig. 3). The enzyme is assembled as a trimer of dimers, with two distinct modes of interaction between subunits. The dimer pairs are related by a threefold symmetry axis running through the central channel and perpendicular to the view in Fig. 3(*a*), and each dimer is formed about a twofold axis perpendicular to this threefold axis. The interactions between the more tightly associated subunits in the dimers, such as subunits *A* and *F* in Fig. 3(*a*), lead to the burial of 3565 $Å^2$ of otherwise accessible surface area. The interface between adjacent dimer pairs, such as subunits *A* and *D*, is less extensive and involves only 2383 $Å^2$ of buried surface area.

Each interface in the dimer creates two active sites, with the bound inosine molecules separated by 25 Å (Fig. 3*b*). The active centre itself can be divided into a nucleoside binding site and a sulfate binding site below it (Fig. 2*c*), with the sulfates of a dimer pair separated by 21 Å.

3.3.2. Intersubunit interactions. Residues that form intersubunit hydrogen bonds are listed in Table 3. The loop that connects strand β_7 and helix α_6 participates in intersubunit interactions close to the central channel in the hexamer and is particularly

striking. It comprises residues Tyr161–Arg169 and extends across the neighbouring subunit in the dimer. The hydrogen bond that is formed between Tyr161 of chain *A* and Glu77 of chain *F* has also been described for *T. thermophilus* PNP (*Tt*PNP; Tahirov *et al.*, 2004). This interaction seems to be conserved, since a sequence comparison of PNPs from *E. coli* (*Ec*PNP), *H. pylori* and *B. subtilis* (Kicska, Tyler, Evans, Furneaux, Kim *et al.*, 2002) shows that both Glu and Tyr are conserved at these positions and both residues are also found in the MTAP sequence of *S. solfataricus* (Appleby *et al.*, 2001). However, relative to PNP from *T. thermophilus* and *E. coli*, the *Pf*PNP β_7-α_6 loop is longer and reaches towards the next-but-one subunit in the adjacent dimer with a closest main-chain approach of 6 Å between Ile165 in chain *A* and Asp172 in chain *C*. Superposition of the PNP monomers from *P. falciparum*, *E. coli* and *T. thermophilus* highlights the different lengths of this loop (Fig. 4). This loop in *Pf*PNP extends 5.7 Å further from the core of the subunit relative to *Ec*PNP and 11.3 Å further compared with *Tt*PNP. This loop also flanks the ligand found in the *Pf*PNP–ino structure. Thus, we propose that the elongated *Pf*PNP β_7-α_6 loop is well positioned to play an important role in both the formation of the hexameric quaternary structure found in bacterial and the *Plasmodium* PNPs and in determining the accessibility and conformation of the active-site cavity.

Since the active site is located at the dimer interface, the substrate can also contribute significantly to intersubunit

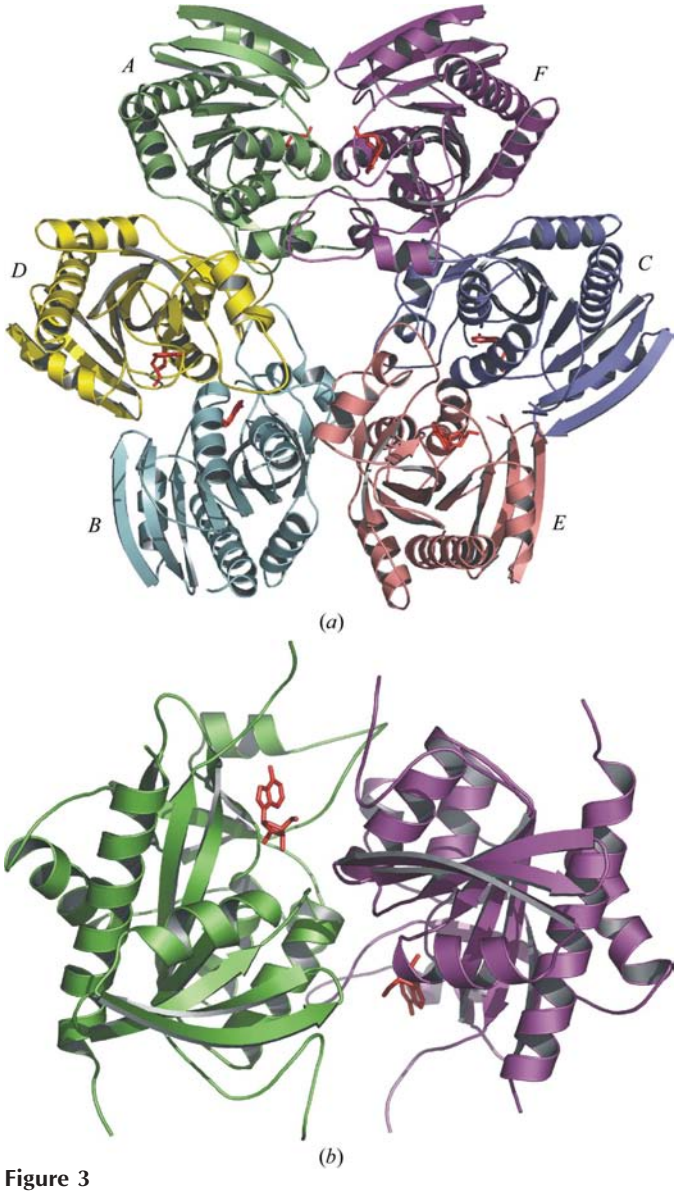

Figure 3
(*a*) Ribbon diagram of the *Pf*PNP hexamer with individual subunits coloured and with bound inosine molecules in liquorice representation (red). The hexamer was generated by application of crystallographic symmetry operations. The view is approximately down the threefold axis. (*b*) A *Pf*PNP–ino dimer pair corresponding to subunits *A* and *F* with the active sites facing each other. The view is approximately down the twofold axis.

Table 3
Representative intersubunit hydrogen bonds of the *Pf*PNP–ino hexamer.

Reciprocal interactions between $F \rightarrow A$ and $D \rightarrow A$ are identical owing to symmetry and are not listed. These interactions are mirrored in the other subunits of the hexamer.

(*a*) $A \rightarrow F$ interactions.

Subunit *A*	Subunit *F*	Distance (Å)
Arg6 $N^{\eta 1}$	Tyr160 O^{η}	2.40
His7 $N^{\varepsilon 2}$	Ino O5′	2.76
Glu46 $O^{\varepsilon 2}$	Val66 NH	2.32
Glu77 $O^{\varepsilon 1}$	Tyr161 O^{η}	2.74
Asp115 C═O	Arg116 $N^{\eta 1}$	2.51
Arg116 $N^{\eta 1}$	His119 $N^{\varepsilon 2}$	3.22
Leu120 C═O	Asn163 $N^{\delta 2}$	2.41

(*b*) $A \rightarrow D$ interactions.

Subunit *A*	Subunit *D*	Distance (Å)
Arg113 NH	Asp125 C═O	2.93
Arg113 C═O	Asp125 $O^{\delta 1}$	2.87
His123 $N^{\varepsilon 2}$	Asp172 $O^{\delta 2}$	2.55
Asn177 $N^{\delta 2}$	Leu194 C═O	3.09
	Thr193 C═O	2.91

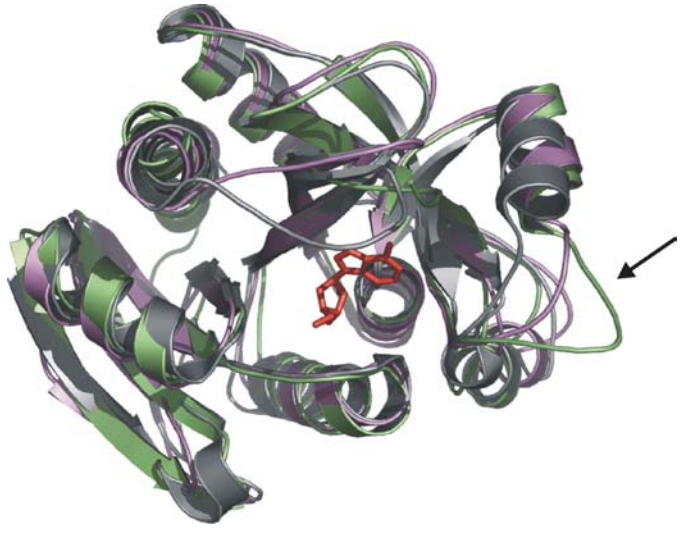

Figure 4
Superposition of PNPs from *E. coli* (violet), *T. thermophilus* (grey) and *Plasmodium* (light green) with inosine bound. The arrow marks the loop that is more extended in *Pf*PNP than in either *Ec*PNP or *Tt*PNP.

interactions. The 5′-hydroxyl group of the inosine ribose ring is within hydrogen-bonding distance of N^{ε} of the imidazole of His7′ from the neighbouring subunit. Again, this interaction is conserved among PNP structures. Another conserved interaction is a salt bridge formed between Arg45 and the sulfate/phosphate bound in the adjacent subunit (Mao *et al.*, 1997; Shi *et al.*, 2004; Tahirov *et al.*, 2004). Substitution of this residue results in loss of activity (Hershfield *et al.*, 1991). In *Pf*PNP–ino, Arg45 takes up the same position as in the sulfate-complexed PNP structure, with an orientation towards the adjacent subunit.

3.4. Active site

The two PNP structures presented here provide insight into how the nucleoside and the phosphate are bound in the active site. Co-crystallization with inosine was carried out in the absence of phosphate, which would have led to glycosidic bond cleavage and release of the products hypoxanthine and ribose-1-phosphate (Fig. 1). The sulfate which is bound to the second structure occupies the putative phosphate-binding site in the active centre. For a better understanding of ligand-binding mechanisms and probable reorientations of residues at different catalytic stages, the *Pf*PNP–immucillin structure (PDB code 1nw4) representing the transition state of the enzyme reaction was superimposed with *Pf*PNP–ino (r.m.s.d. 0.43 Å) and *Pf*PNP–SO_4 (r.m.s.d. 0.30 Å). Superposition was carried out by least-squares procedures applied to the enzyme's C^{α} atoms.

In the overall view of the model as it is shown in Figs. 2(*c*) and 3(*b*), the β-barrel structure forms the back of the nucleoside-binding site which opens onto the subunit interface of the dimer pair. The ligand is flanked by the extended loop β_7-α_6 on one side. The phosphate-binding site below the ligand is located at the interface of the β-sheet/β-barrel structure.

3.4.1. Nucleoside-binding site. The stereo image of the *Pf*PNP–ino active site in Fig. 5 reveals the hydrophobic environment of the nucleoside, where the inosine base is oriented by π-stacking and van der Waals interactions. Glu184 and His7′ (*i.e.* from the adjacent subunit) form hydrogen bonds to the ribose, as in the *Pf*PNP–immucillin structure. In *Pf*PNP–ino, Ser91 is also within hydrogen-bonding distance of atom O4 of the ribose ring, whereas in *Pf*PNP–immucillin this residue forms a polar interaction with the bound sulfate.

Although the active-site stereochemistry is generally well preserved, the superposition reveals some differences between *Pf*PNP–ino and *Pf*PNP–SO_4 surrounding the binding site of the nucleoside base (Fig. 6). The most striking difference is in the position of the catalytic residue Asp206, whose protonated side-chain carboxylate forms a hydrogen bond with the purine N7

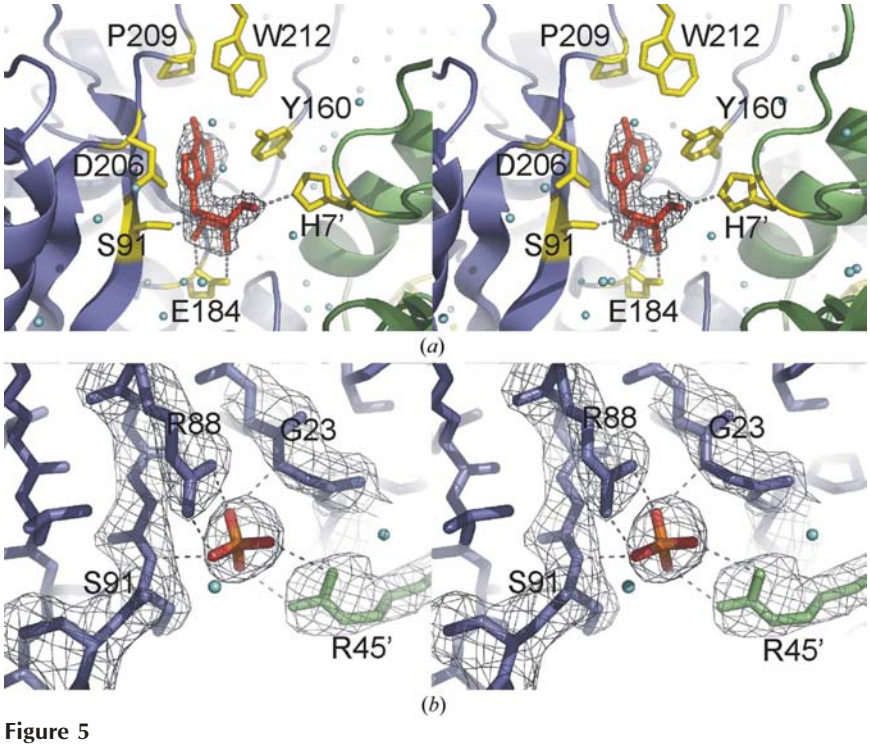

Figure 5
Stereo images of the active site of *Pf*PNP–ino and *Pf*PNP–SO_4. (*a*) Inosine-binding pocket of *Pf*PNP. The inosine ligand is in red, while the enzyme is displayed in ribbon representation and coloured by subunit with selected protein side chains coloured in yellow and labelled. Waters are shown in cyan. Enzyme–substrate hydrogen-bonding interactions are shown as dashed lines. The electron density associated with the inosine ligand is an omit map contoured at 0.7σ. (*b*) Phosphate-binding pocket. The stick model is coloured by subunit with the bound sulfate in orange/red. The $2F_o - F_c$ electron density contoured at 1.2σ is displayed on the sulfate and surrounding residues. Residues that form salt bridges and hydrogen bonds with the sulfate are labelled.

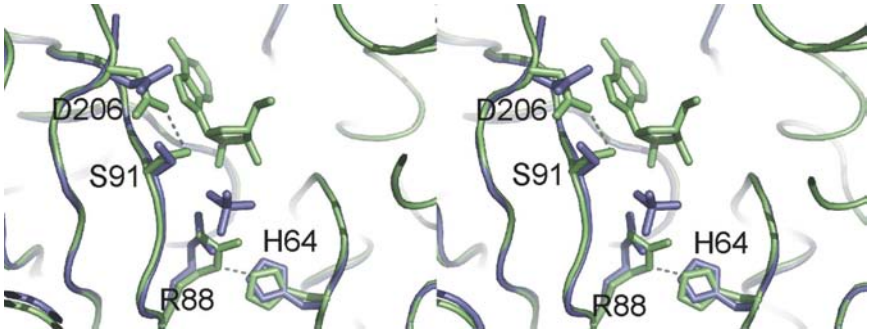

Figure 6
Stereoview of the superposed structures of *Pf*PNP–ino and *Pf*PNP–SO_4. *Pf*PNP–ino (light green) and *Pf*PNP–SO_4 (blue) are displayed as cartoons. The residues that undergo changes in orientation are shown as stick models. Asp206 interacts with Ser91 in *Pf*PNP–ino, while in *Pf*PNP–SO_4 Asp206 is oriented further away from the nucleoside-binding site. Arg88 is hydrogen bonded to sulfate, but is shifted when the sulfate-binding site is empty (as in *Pf*PNP–ino) and interacts with His64 instead.

during phosphorolysis (Shi *et al.*, 2004; Koellner *et al.*, 2002). In the sulfate-bound structure the carboxylate of Asp206 is oriented away from the empty purine-binding site, while in the *Pf*PNP–ino model the C^{γ} atom of this residue is 1.4 Å closer to the nucleoside. Even so, the Asp206 carboxylate to purine N7 distance is much longer (3.8 Å) than the corresponding distance in the *Pf*PNP–immucillin complex (2.8 Å) where an enzyme–inhibitor hydrogen bond is formed (Fig. 7). This argues that the carboxylate–base interaction is exclusive to the enzyme–transition state complex and not critical for initial substrate binding. Instead of forming a hydrogen bond with the substrate in the *Pf*PNP–ino complex, Asp206 appears to form a hydrogen bond (2.8 Å) with the Ser91 hydroxyl (Fig. 6). However, the electron density around Ser91 suggests a possible alternate conformation, with one conformer facing towards Asp206 and the other interacting with the ribose ring of inosine.

Superposition of the *Pf*PNP–ino and *Pf*PNP–immucillin structures shows a 0.8 Å shift in the position of O6 of the purine base and 0.7 Å in the position of N7 (Fig. 7). In the immucillin-H complex, more residues, in particular Asp206, are involved in orienting the ligand, presumably as part of transition-state stabilization. Trp212, for example, forms water-mediated contacts with the 6-oxo group of immucillin-H and Asp206. In the *Pf*PNP–ino structure this contact is not formed, since Trp212 as well as Tyr160 are shifted in concert with the substrate (Fig. 7). The implied movement of the main chain at Trp212 between ground-state and transition-state structures is consistent with the proximity of this residue to the flexible loop region.

3.4.2. Phosphate/sulfate-binding site. In the PNP–immucillin structure, residues Gly23, Arg88, Ser91 and Arg45′ form hydrogen bonds with the sulfate bound beneath the inhibitor. The same residues are also involved in forming bonds with the sulfate ion in *Pf*PNP–SO_4 (Fig. 5). The positions of the sulfate molecules in the *Pf*PNP–SO_4 and the immucillin-bound *Pf*PNP structure are remarkably similar, with the sulfate S atoms displaced by a mere 0.16 Å (with an r.m.s.d. of 0.34 Å for all five sulfate atoms) following superposition of all equivalent C^{α} atoms. The most striking conformational difference at the (unoccupied) phosphate/sulfur-binding site occurs at Arg88 of the *Pf*PNP–ino model, where the side chain is oriented so that it forms a hydrogen bond to His64 (Fig. 6). Since the other residues that interact with sulfate show few significant reorientations in the *Pf*PNP–ino structure, residue Arg88 may be an important mediator of conformational changes when sulfate/phosphate binds to the active site.

3.4.3. Flexible loop. A structural feature that may play a crucial role in substrate binding and catalysis is hinted at by the main-chain discontinuity between strand β_9 and helix α_8 in both of the *Pf*PNP structures presented here, indicating the presence of a flexible loop. The disordered regions span residues 215–220 in *Pf*PNP–ino and 208–223 in *Pf*PNP–SO_4. In the immucillin-bound PNP structure, this loop is well defined in the electron-density maps, which show that it forms a kind of lid over the substrate-binding pocket (Fig. 7). This loop conformation is stabilized by a network of hydrogen bonds with the purine moiety of the tightly bound inhibitor, which would explain why the disordered segment in the nucleoside-free *Pf*PNP–SO_4 structure is even larger than in the inosine-bound structure. In the immucillin structure there is a water-mediated interaction between Asp206 and Asp218 of the loop region (Fig. 7), a bond that does not form when Asp206 is shifted away from the binding pocket as in *Pf*PNP–SO_4 or when Asp206 interacts with Ser91 as in the *Pf*PNP–ino structure. A similar disorder to order transition of this loop accompanying ligand binding was observed for the *T. thermophilus* structure (Tahirov *et al.*, 2004).

3.4.4. Comparison with the transition-state *Pf*PNP structure. The two new structures presented here can be jointly considered as an image of the binding of substrates just prior to engaging the enzymatic reaction. We can thus compare the key distances implicated in the formation of the proposed oxycarbenium ion intermediate: the distance between the inosine C1′ atom and the most proximal sulfate O atom (Tahirov *et al.*, 2004). In the resulting hypothetical bisubstrate–enzyme complex this distance is 3.8 Å, whereas the corresponding distance in the immucillin-bound transition-state structure is 3.3 Å (Shi *et al.*, 2004). Interestingly, this suggests that during the reaction the nucleoside is moving toward the phosphate/sulfate position rather than *vice versa*, since the position of the sulfates in the *Pf*PNP–SO_4 and in the immucillin-bound *Pf*PNP structures are so similar (Fig. 7).

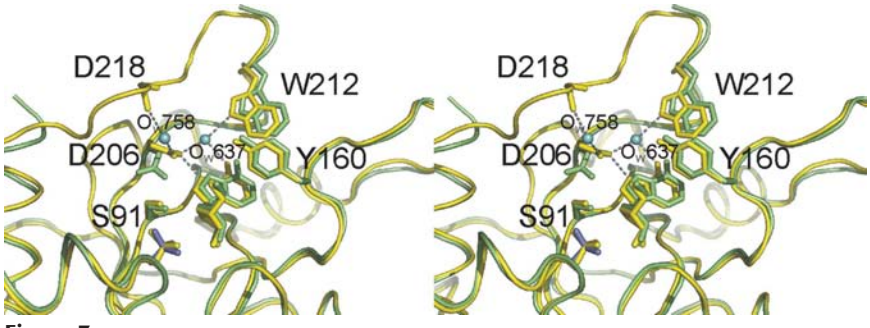

Figure 7
Stereoview of the superposition of *Pf*PNP–ino (light green), *Pf*PNP–SO_4 (only the sulfate is shown, in blue) and *Pf*PNP–immucillin (yellow). The loop above the binding pocket of the immucillin-H complex structure is complete and shows a water-mediated bond between residues Asp218 and Asp206, whereas in the other two structures the loop is disordered or flexible and the model cannot be built. The *Pf*PNP–immucillin structure shows a water-mediated interaction of Asp206 and Trp212 with the inhibitor. In *Pf*PNP–ino, the substrate does not form these bonds and is shifted relative to immucillin-H, together with the aromatic residues Trp212 and Tyr160.

3.5. Structural features of the malarial PNP compared to other PNPs

The two malarial PNP structures presented here reveal critical structural features that might help the further elucidation of the catalytic mechanism of this enzyme. The first is the flexibility of Asp206,

a residue that forms a hydrogen bond with the transition-state analogue, but is differently oriented when the inosine substrate is bound or when the binding site is empty. Movement of the corresponding Asp (204) in *Ec*PNP has also been reported: ten *Ec*PNP purine nucleoside complexes were characterized and it was found that although good substrates did not always show an Asp204–N7 bond in the structures, mutation studies proved that the residue is critical for catalysis (Bennett *et al.*, 2003). This implied that Asp204 is not essential for substrate binding and that it can move in concert with the substrate during catalysis to donate a proton to N7 as the glycosidic bond breaks. After protonating the nucleoside base, Asp204 forms a salt bridge with Arg217 (Koellner *et al.*, 2002), which again indicates that this residue is flexible.

The second structural feature of the malarial PNP is the flexibility of the β_9-α_8 loop. In *Ec*PNP, the helix corresponding to *Pf*PNP α_8 is thought to play an important conformational role, switching between continuous and segmented conformations and thus controlling access of the substrate to the binding pocket (Koellner *et al.*, 2002). In the *Pf*PNP structures presented here, as well as in the immucillin-bound *Pf*PNP, the conformation of this helix is invariant. This indicates that access to the active site in the *Plasmodium* enzyme may be controlled in a different way to that proposed for *Ec*PNP.

A loop that serves as a gate was likewise described for human PNP, where residues 241–260 move upon substrate binding and the gate movement even involves a helical transformation (De Azevedo *et al.*, 2003). This loop is equivalent to the flexible loop of *Pf*PNP, though it is more extended. From crystal structures of *E. coli* uridine phosphorylase, the swinging movement of a flap region (residues 224–234) was detected that seals the active site (Caradoc-Davies *et al.*, 2004). Hence, flexibility near the active site is a common feature of PNPs even though there are differences in its manifestation between enzymes of different origin.

The third feature of the *Pf*PNP that differs from other hexameric PNPs is the extended loop β_7-α_6, which is located on the same side of the disc-shaped hexamer as the flexible loop β_9-α_8. The *Pf*PNP structures suggest that this loop not only contributes to intersubunit contacts, but also could plausibly form an additional gate controlling the access of substrates to the active site.

This work was funded by the Wellcome Trust (grant No. 066742/F/01/Z) and the NIGMS (grant No. 1P50-GM64655-01 to WGJH). The European Synchrotron Radiation Source (Grenoble, France) and the Advanced Light Source (Berkeley, CA, USA) are thanked for the provision of X-ray data-collection facilities. The authors thank Sue Kyes (Molecular Parasitology Group, The Weatherall Institute of Molecular Medicine, University of Oxford, UK) who provided genomic DNA of *P. falciparum* 3D7 and Andrew Leech (Technology Facility, Department of Biology, University of York, UK) who carried out the AUC experiments. We also thank many members from the Structural Genomics of Pathogenic Protozoa (SGPP) project (http://www.sgpp.org) for valuable contributions, including Frank Zucker, Thomas Earnest, Erica Boni, Peter Myler, Christophe Verlinde, Wes Van Voorhis, Fred Buckner, Michael Gelb, Martin Criminale, Larry DeSoto, Oleksandr Kalyuzhniy, George DeTitta, Angela Lauricella, Stacy Gulde, Lori Schoenfeld, Elizabeth Grayhack, Eric Phizicky, J. T. Reddy and Erkang Fan.

References

Appleby, T. C., Mathews, I. I., Porcelli, M., Cacciapuoti, G. & Ealick, S. E. (2001). *J. Biol. Chem.* **276**, 39232–39242.
Asahi, H., Kanazawa, T., Kajihara, Y., Takahashi, K. & Takahashi, T. (1996). *Parasitology*, **113**, 19–23.
Bennett, E. M., Li, C., Allan, P. W., Parker, W. B. & Ealick, S. E. (2003). *J. Biol. Chem.* **278**, 47110–47118.
Burling, T., Kniewel, R., Buglino, J. A., Chadna, T., Beckwith, A. & Lima, C. D. (2003). *Acta Cryst.* D**59**, 73–76.
Caradoc-Davies, T. T., Cutfield, S. M., Lamont, I. L. & Cutfield, J. F. (2004). *J. Mol. Biol.* **337**, 337–354.
Collaborative Computational Project, Number 4 (1994). *Acta Cryst.* D**50**, 760–763.
De Azevedo, W. F., Canduri, F., Dos Santos, D. M., Silva, R. G., De Oliveira, J. S., De Carvalho, L. P. S., Basso, L. A., Mendes, M. A., Palma, M. S. & Santos, D. S. (2003). *Biochem. Biophys. Res. Commun.* **308**, 545–552.
DeLano, W. L. (2002). *The PyMOL Molecular Graphics System.* DeLano Scientific, San Carlos, CA, USA. http://pymol.sourceforge.net/.
Hassan, H. F. & Coombs, G. H. (1988). *FEMS Microbiol. Rev.* **4**, 47–83.
Hershfield, M. S., Chaffee, S., Koro-Johnson, L., Mary, A., Smith, A. A. & Short, S. A. (1991). *Proc. Natl Acad. Sci. USA*, **88**, 7185–7189.
Herzberg, O. & Moult, J. (1991). *Proteins*, **11**, 223–229.
Howlin, B., Butler, S. A., Moss, D. S., Harris, G. W. & Driessen, H. P. C. (1993). *J. Appl. Cryst.* **26**, 622–624.
Kicska, G. A., Tyler, P. C., Evans, G. B., Furneaux, R. H., Kim, K. & Schramm, V. L. (2002). *J. Biol. Chem.* **277**, 3219–3225.
Kicska, G. A., Tyler, P. C., Evans, G. B., Furneaux, R. H., Schramm, V. L. & Kim, K. (2002). *J. Biol. Chem.* **277**, 3226–3231.
Koellner, G., Bzowska, A., Wielgus-Kutrowska, B., Luic, M., Steiner, T., Saenger, W. & Stepinski, J. (2002). *J. Mol. Biol.* **315**, 351–371.
Mao, C., Cook, W. J., Zhou, M., Koszalka, G. W., Krenitsky, T. A. & Ealick, S. E. (1997). *Structure*, **5**, 1373–1383.
Murshudov, G. N., Vagin, A. A. & Dodson, E. J. (1997). *Acta Cryst.* D**53**, 240–255.
Otwinowski, Z. & Minor, W. (1997). *Methods Enzymol.* **276**, 307–326.
Parker, W. B., King, S. A., Allan, P. W., Bennett, L., Secrist, J. A., Montgomery, J. A., Gilbert, K. S., Waud, W. R., Wells, A. H., Gillespie, G. Y. & Sorscher, E. J. (1997). *Hum. Gene Ther.* **8**, 1637–1644.
Perrakis, A., Morris, R. & Lamzin, V. S. (1999). *Nature Struct. Biol.* **6**, 458–463.
Pugmire, M. J. & Ealick, S. E. (2002). *Biochem. J.* **361**, 1–25.
Shi, W., Ting, L., Kicska, G. A., Lewandowicz, A., Tyler, P. C., Evans, G. B., Furneaux, R. H. & Schramm, V. L. (2004). *J. Biol. Chem.* **279**, 18103–18106.
Suh, K. N., Kain, K. C. & Keystone, J. S. (2004). *Can. Med. Assoc. J.* **170**, 1693–1702.
Tahirov, T. H., Inagaki, E., Ohshima, N., Kitao, T., Kuroishi, C., Ukita, Y., Takio, K., Kobayashi, M., Kuramitsu, S., Yokoyama, S. & Miyano, M. (2004). *J. Mol. Biol.* **337**, 1149–1160.
Terwilliger, T. C. & Berendzen, J. (1999). *Acta Cryst.* D**55**, 849–861.
Vagin, A. A. & Teplyakov, A. (1997). *J. Appl. Cryst.* **30**, 1022–1025.
Van Duyne, G. D., Blandaert, R. F., Karplus, P. A., Schreiber, S. L. & Clardy, J. (1993). *J. Mol. Biol.* **229**, 105–124.